Electrochemical Evaluation of Fluorinated MnO_2 for Supercapacitor Application

Siti Nur Najwa Mohd Yusof[1], *Nurul Khairiyyah* Mohd Zain[1], *Izan Izwan* Misnon[1,*] and *Rajan* Jose[1]

[1]Nanostructured Renewable Energy Materials Laboratory, Faculty of Industrial Sciences & Technology, Universiti Malaysia Pahang, 26300 Gambang, Kuantan, Pahang, Malaysia

Abstract. Supercapacitors (SCs) functioning as alternative energy storage is useful in most electronic devices, renewable energy system and hybrid vehicles that have high demand in these days. Excellent electrochemical performance, environment friendliness and low cost material are needed to fulfil the energy demand by most developed country. In this study, fluorination treatment on manganese oxide (MnO_2) is considered as an effective way to develop better energy storage due to fluorine electronegativity and reactivity when correlate with other element. Hydrothermal method is used to synthesis MnO_2 (α–MnO_2 and δ–MnO_2) and the effect of fluorination (F–α–MnO_2 and F–δ–MnO_2) on MnO_2 surfaces is investigated on the charge storage ability. The crystallinity and functional groups of the samples was confirmed by the X-ray diffractogram and fourier transforms infrared spectroscopy (FTIR). The cyclic voltammetry (CV) and galvanostatic charging–discharging (CDC) analysis in 0.5 M K_2SO_4 electrolyte shows that F-δ-MnO_2 gives the highest *Cs* value of 184 F g^{-1} at scan rate of 5 mV s^{-1} and 66 F g^{-1} at current density of 0.3 A g^{-1}. The electrochemical impedance spectroscopy shows that the F–δ–MnO_2 has the lowest electrode resistances and charge transfer resistance which contributes to high *Cs* and the high conductivity of electrode.

1 Introduction

Electrochemical capacitors which known as supercapacitors (SCs), are compatible for application such as hybrid vehicles, portable electronic devices and renewable energy system that require high charge–discharge rates and high power density [1]. This is owing to their excellent power densities than conventional batteries (eg: lithium ion batteries), high charge and discharge rate also have long life cycles which is up to 10^4 cycles [1]. In accordance to charge storage mechanisms, SCs could be categorized into two types which are electrochemical double layer capacitors (EDLCs) and pseudocapacitors (PCs). The EDLCs operate on surface absorption at the electrode materials and electrolyte interfaces. Numerous carbon materials such as carbon aerogels, graphene and mesoporous carbons with high surface area have been used as electrode materials for SCs [2]. The PCs are based on faradaic redox reactions which occur at the electrode surfaces and its bulk fragment. Transition-metal oxides (TMOs), hydroxides, chalcogenides (eg: RuO_2, MnO_2, Co_3O_4, $Ni(OH)_2$ and MoS) and conducting polymers (eg:polypyrrole and polythiophenes) basically shows pseudocapacitive behavior. Basically, the PCs have much greater capacitance compared to the EDLCs.

Tremendous effort have been done by researchers in order to improve energy and power densities of the device using TMOs due to their availability along with multiple electron transfer and variable oxidation states during faradaic reactions [2,3]. Among TMOs, MnO_2-based electrodes are considered as most preferable for SCs fabrication due to their environmental friendly, natural abundance, low cost, wide potential window, and good electrochemical performance compared to RuO_2 electrode which is limited by its high cost and low abundance [2,4–7]. Manganese oxides can be existed in several allotropes including α, β, γ, δ, and λ due to the different arrangement of linkage of the basic [MnO_6] octahedral unit. The α, β, and γ-type MnO_2 exhibit 1D tunnel structure, whereas δ-type MnO_2 shows a 2D layered structure [8].

Several methods was used to synthesis MnO_2 including precipitation, self-reacting microemulsion, hydrothermal methods, sonochemical and room-temperature solid reaction. Among this, hydrothermal method is considered as the most popular synthesis approaches to synthesize numerous forms of MnO_2 and gives many advantages includes a wide range of initial precursors and mild synthesis conditions such as temperature and pH can be used. A solvothermal or hydrothermal method has been engaged to prepare one-dimensional nanoscaled materials, for instance, α-MnO_2, without using catalysts or templates. This method is remarkable to traditional methods since the equipment required is not particular and expensive for the preparation of nanostructured materials at a low

* Corresponding author: iezwan@ump.edu.my.

temperature. Preparation of MnO_2 by hydrothermal method is generally involve the phase transformation of granular MnO_2 precursors or redox reactions of MnO_4^- and/or Mn^{2+}[9]. Layered MnO_2 structure can be obtained by chemical treatments of Mn ions in a basic solution [10].

Zhang et al reported that, a layered structure of mesoporous birnessite-type manganese oxide (δ-MnO_2) with large specific surface area (SSA) consists of pores on nanometer scale and bicontinuous networks of solid become an attractive allotrope for active electrode material [5]. Commonly, specific capacitance (C_S) of the cathode materials is associated to ionic transport within the pores, electrical conductivity in the solid phase and its specific surface area. Therefore, α-MnO_2 and δ-MnO_2 is acceptably to be chosen electrodes for high-performance SCs due to their crystallographic structure and accessible nanostructures where MnO_2 with high C_S, low fabrication cost and good cyclic stability are expected [8].

Fluorination treatment is the best method to improve electrode performances because fluorine is the most reactive and most electronegative correlate with other elements. As a result, when fluorine is combined with the other element, it will forms stronger bonds by attracting more ions towards it. Kim et al. reported on fluorinated activated carbon (ACs) which shows improving capacitance performance compared to raw ACs due to its semi-ionic bonding character between AC and fluorine [1,9]. The potential of fluorination on TMOs is still lacking in the energy storage field. Hence in this research, the main target is the study of fluorination treatment on α-MnO_2 and δ-MnO_2 surface as well as to examine the effect to its capacitance.

2 Experimental

2.1 Material synthesis

The MnO_2 structures were synthesized using hydrothermal method. In this experiment, two samples were prepared using different precursor to oxidant ratio, 1:1 for α-MnO_2 and 1:6 for δ-MnO_2. The α-MnO_2 is prepared by dissolving $KMnO_4$ (0.05 mol) in 100 ml of deionized water. Then, the mixture is added with (0.05 mol) ammonium persulfate ($NH_4S_2O_8$). Next, the solution is stir for about 30 minutes and place in the Teflon-lined stainless steel reactor. The sample was heated in an oven for 24 hours at the temperature of 90 °C. After that, the reactor is cooled down to room temperature and then the brownish precipitate that produced is filtered. The sample is washed using deionized water followed by ethanol. The brownish precipitate is then dried for 24 hours at 50 °C. The fluorination of MnO_2 series was carried out by immersion into 50 mL of ammonium hexafluorosilicate [$(NH_4)_2SiF_6$] solution for 30 minutes. Next, the slurry was separated by filtration, washed clean using distilled water and then dried it at 110 ˚C for 24 hours to produce F-α-MnO_2 and F-δ-MnO_2.

2.2 Material characterization

The manganese dioxide structures were characterized by a range of characterization techniques such as XRD, FTIR, FESEM, EDAX and BET to find their crystals structure, molecular structures, topographical and elemental information, surface area and electrical properties.

2.3 Electrode fabrication and electrochemical evaluation

The MnO_2 sample is mixed with conducting carbon and polyvinylidene fluoride (PVDF) in the mass ratio of 80:10:10 in glass vial. Few drops of N-methyl-2-pyrrolidinone (NMP) was added into the mixture and stirred for 8 h to produce homogeneous slurry. The obtained slurry was coated onto nickel (Ni) foam current collector with an effective area of ~1 cm^2 by using brush technique and dried at 70 °C in the oven for 24 h. After that, the electrode was pressed at 5 MPa to produce better active material in contact with current collector.

Cyclic voltammetry (CV) were carried out in the potential range of 0.0–1.0 V at different scan rates of 2–100 mV s^{-1} for all electrodes with respect to Ag/AgCl as a reference electrode in 0.5 M K_2SO_4.The C_S of the electrodes were calculated from the CV curve using Equation 1.

$$C_S = \frac{1}{2mv(E_2-E_1)} \int_{E_1}^{E_2} i(E)dE \quad (1)$$

where m is the mass of the active material, v is the scan rate, E_2–E_1 gives the potential window, and $i(E)$ is the current at each potential.

Galvanostatic charge discharge (CDC) was obtained in the potential range 0.0–1.0 V at different current density (0.3, to 10.0 A g^{-1}) in 0.5 M K_2SO_4 electrolyte. The Cs from the discharge curves can be calculated using the Equation 2.

$$Cs = \frac{Ixt}{mx\Delta v} \quad (2)$$

where I, t, m and Δv are applied current, discharge time, active mass and potential difference, respectively.

The electrochemical impedance spectroscopy (EIS) which illustrate the relationship between imaginary and real resistance is conducted in the frequency range of 100 kHz – 10 mHz determines the bulk resistance (R_S), charge transfer resistance (R_{ct}) and ion diffusion resistance (R_d).

3 Results and Discussion

3.1 Material analysis

Figure 1 shows the XRD patterns of all synthesized MnO_2 powders which are α-MnO_2, δ-MnO_2, F-α-MnO_2 and F-δ-MnO_2. The main characteristic peak of α-MnO_2 (Fig. 1a) at 2θ = 12.9, 18.2, 28.8, 37.7, 42.1, 49.8, 55.9,

60.2, 65.5, 69.5 and 73.0°which indexed to formation of pure tetragonal phase of α-MnO_2 with space group of *I*4/*m* (JCPDS 44-0141) [11]. The unit cell parameter of α-MnO2 are a= 9.73 Å, b= 1.3062 Å and c= 2.847Å. The prepared α-MnO_2 has a good crystallinity as it clearly illustrates sharp and clear diffraction peak [13]. The δ-MnO_2 is clearly demonstrated to be a layered structure consisting distinct peaks which correspond to long range of crystalline order in the compound. However, the peaks in Fig. 1b showing that the pattern was similar with previous MnO_2 sample as both pyrolusite and α-MnO_2 phase were present at each peaks. This could be due to excessive heat and reaction during δ-MnO_2 sample preparation. Nayak et al. suggest that it might be the H_2O was expelled from the interlayer gap of δ-MnO_2 which changed the structure into tunneled α-MnO_2 structure [14]. The peak present in Fig. 1c is highly crystalline tetragonal phase of F-α-MnO_2 which confirmed by the formation of peaks at 2θ = 12.63, 17.82, 26.13, 28.54, 36.51, 37.444 and 68.97° with space group P42/mnm (JCPDS card no. 041-1445). The phase present at each peak is α-MnO_2 and manganese fluoride phase. Similarly in Fig. 1d, manganese fluoride present at the peak with addition of pyrolusite phase with same space group of P42/mnm.

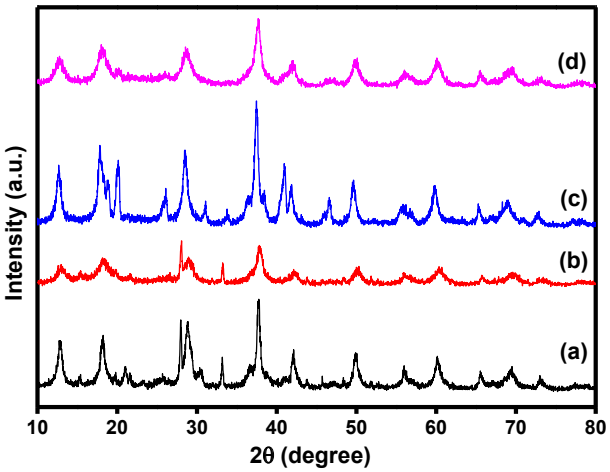

Fig. 1. X-ray diffraction pattern of (a) α-MnO_2, (b) δ-MnO_2, (c) F-α-MnO_2 and (d) F-δ-MnO_2.

The infrared spectra in Fig. 2 show all synthesized MnO_2 have the same absorbance peaks pattern. In the wavelength range of 3700-3000 cm^{-1} regions, the broad peak corresponds to stretching vibrations were recorded and attributed to the hydroxyl group on the MnO_2 surface. The peak detected at range of 1600 cm^{-1} indicate the bending vibration of water molecules whereas at wavelength of 1400 cm^{-1} are correlated with hydration of water and bending of Mn-OH in MnO_2 sample [15]. The band centered at ~1100 cm^{-1} correspond to bending and absorption of the Mn-OH functional groupand peaks at ~700 cm^{-1} attribute to the characteristics peak of manganese oxide. The IR result proposed the presence of water bonded in all of the MnO_2 structure, which responsive to the electrochemical activity of the material [16]. The IR result indicates the presence of some bound water in the sample. The fluorine vibration is not detectable using this technique due to low element loading.

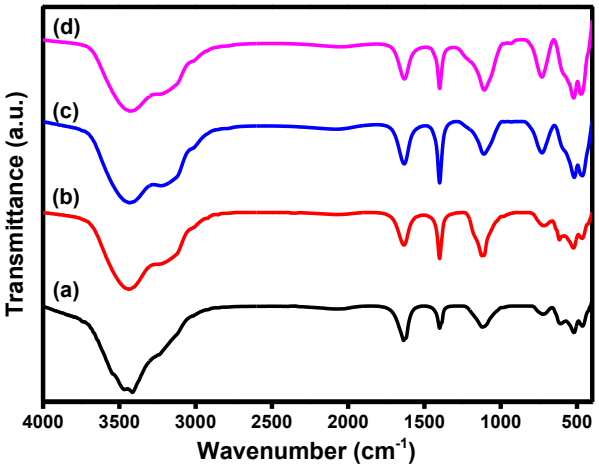

Fig. 2. FTIR spectra of (a) α-MnO_2, (b) δ-MnO_2, (c) F-α-MnO_2 and (d) F-δ-MnO_2 in the region of 4000-400 cm^{-1}.

The morphology of MnO_2 sample was observed using FESEM at low and high magnification as shown in Fig. 3. The image at low magnification (Fig. 3a) illustrates wool-like morphology while at high magnification the sample of α-MnO_2 showing a bundle of very fine, randomly-oriented needles that are about 80 nm in diameter. Similar morphology is observed for the sample of F-α-MnO_2 (Fig. 3c) that modified with fluorine which is approximately 50 nm in diameter of the needle-like structures. Fluorination will not change the structure of MnO_2 but its electrochemical properties. It can be further explain from the result of the energy-dispersive X-ray spectroscopy (EDAX) (not shown) that shows small proportion of ~11.68 wt% of fluorine followed by 54.00 and 34.32 wt% of oxygen and Mn in the sample. Fluorine was attached to the surface of MnO_2 because of reduction by fluoric acid. The decrease in oxygen content of F-MnO_2 from the pure MnO_2 may be correlated with the substitution of fluorine for oxygen, which largely covered the surface dangling bonds of MnO_2. The morphology of the δ-MnO_2 and F-δ-MnO_2 samples (Fig. 3b&d) showing the combination of spherical and wool morphology with growing needle-like structure onto the surface. This can be correlated with XRD result where there is two phases present in the sample which are pyrolusite and α-MnO_2 for prepared δ-MnO_2 also manganese fluoride and pyrolusite for F-δ-MnO_2. The well grown needle-like structures are ~60 nm in diameter in F-δ-MnO_2 whereas about 50–100 nm in diameter are observed in δ-MnO_2. The weight percentage (wt %) of fluorine is about 9.58 % followed by 26.14 and 64.28 % of Mn and O phase resulting from EDAX analysis.

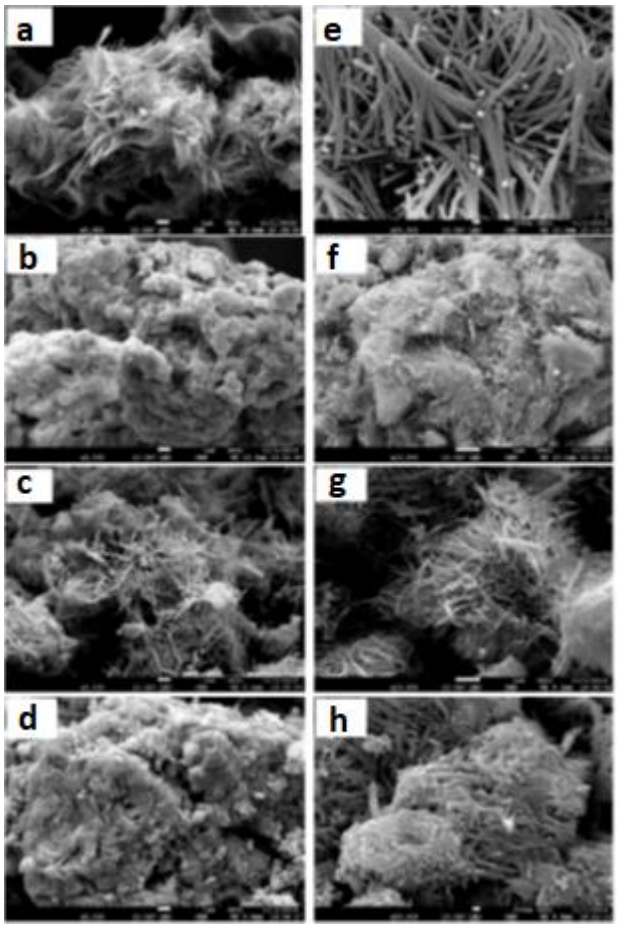

Fig. 3. FESEM morphology at low magnification of (a) α-MnO_2, (b) δ-MnO_2, (c) F-α-MnO_2 and (d) F-δ-MnO_2 and high magnification of (e) α-MnO_2, (f) δ-MnO_2, (g) F-α-MnO_2 and (h) F-δ-MnO_2.

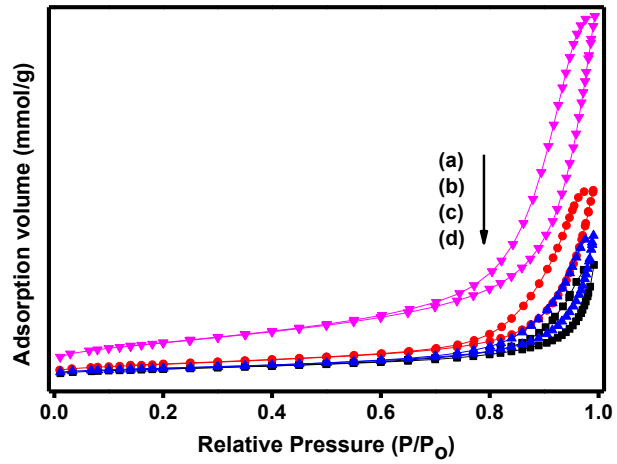

Fig. 4. Nitrogen adsorption-desorption analysis for (a) α-MnO_2, (b) δ-MnO_2, (c) F-α-MnO_2 and (d) F-δ-MnO_2.

Nitrogen adsorption of MnO_2 was measured to determine the specific surface area and pore volume between pure and fluorinated MnO_2 sample. Figure 4 shows the isotherms of α-MnO_2, δ-MnO_2, F-α-MnO_2 and F-δ-MnO_2 which belongs to type IV, showing hysteresis loop that indicates the mesoporous nature of the samples. At higher pressures, the absorption of nitrogen increase as pores was filled. The pore volumes were calculated correspond to Barrett–Joyner–Halenda (BJH) methods. The BET surface area, total pore volume, and average pore diameter for all samples are listed in Table 1. The F-δ-MnO_2 have the highest BET surface area and pore volume which are 121.7574 $m^2 g^{-1}$ and 0.485473 $cm^3 g^{-1}$ compared to the other sample. This indicates fluorinated MnO_2 is more porous than the pure MnO_2 and proved the assumption that fluorinated MnO_2 can exhibit high electrochemical activity. The highly porous structure can shorten the diffusion path for charge-carrier ions, while the large liquid-solid interface can facilitates ion exchange between the electrode and electrolyte.

Table 1. BET analysis of MnO_2 sample.

Sample	BET surface area ($m^2 g^{-1}$)	Total pore volume (cm^3/g)	Average pore size (Å)
α-MnO_2	34.0539	0.133775	181.215
δ-MnO_2	50.2462	0.256872	197.544
F-α-MnO_2	37.1871	0.174289	208.740
F-δ-MnO_2	121.7574	0.485473	160.087

3.2 Electrochemical analysis

Figure 5 shows the CV curves of typical MnO_2 sample at various scan rate. The CV curves illustrate near rectangular-like shape of an ideal pseudocapacitive behavior.

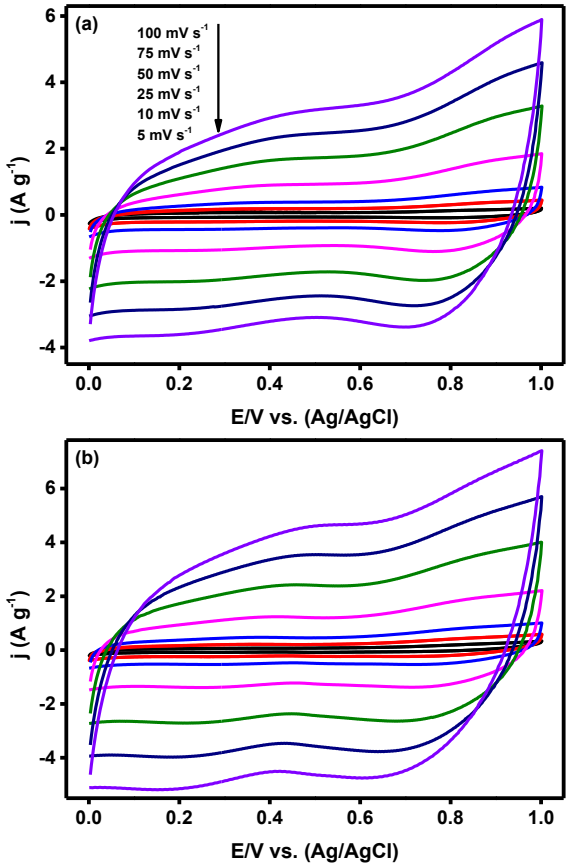

Fig. 5. Typical CV curves of (a) δ-MnO_2, and (b) F-δ-MnO_2 at scan rate of 5 – 100 mV s^{-1}.

The C_S obtained from the CV curves are 63, 158, 76 and 184 F g^{-1} for α-MnO_2, δ-MnO_2, F-α-MnO_2 and F-δ-MnO_2 electrodes respectively at the scan rate of 5 mV s^{-1}. The C_S decreases when the scan rate is increases. This is because electron cannot attach at the surface of the electrode because of the fast reaction of scan rate. Basically the utility of cyclic voltammetry is highly dependent on analyte used which has to be redox. If higher scan rate is used, it creates peak with large current and resistance which result in distortions.The result clearly shows that the C_S value is increased in following order: α-MnO_2 < F-α-MnO_2 < δ-MnO_2 < F-δ-MnO_2 which prove that the fluorination treatment on MnO_2 surface can improve the capacitance of the electrode.

Figure 6 represent the galvanostatic charging–discharging (CDC) curves of all samples with potential range of 0.0 – 1.0 V. The C_S at discharge current density of 0.3 A g^{-1} are 25, 50, 23 and 66 F g^{-1} calculated using formula in Eq. 2. In CDC, the higher the current densities cause the lower the C_S value. This result was affected by the value of discharging time. The higher the current density, the shorter the discharging time and causes the C_S to be lowered.

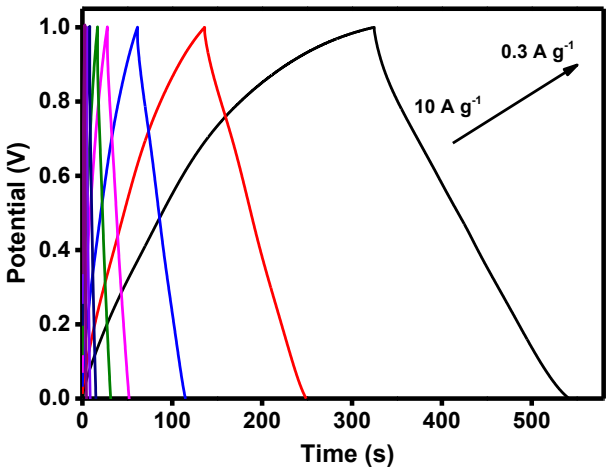

Fig. 6. Typical CDC curves of F-δ-MnO_2 at scan rate range of 0.3 – 10 A g^{-1}.

Figure 7 clearly shows that the C_S value is increase in following order: F-α-MnO_2 < α-MnO_2 < δ-MnO_2 < F-δ-MnO_2. The fluorination treatment on MnO_2 surface should improve the capacitance of the electrode. However the specific capacitance value in fluorinated α-MnO_2 is much smaller than the pure sample. This may be due to incomplete transfer of ion during discharging process.

The Nyquist plot in Fig. 8 illustrate of all sample immersed in 0.5M K_2SO_4 electrolyte which examined at the range of 0.01 to 10 000 Hz. At high frequency region, the resulting plot showed a half semi-circle whereas at low frequency region, a straight line is formed. The bulk resistance (R_S) is determined from the high frequency off-set in the real part of complex impedance of the Nyquist plot. The estimated R_S values are 1.07, 1.08 1.09 and 1.05 Ω for α-MnO_2, δ-MnO_2, F-α-MnO_2, and F-δ-MnO_2, respectively.

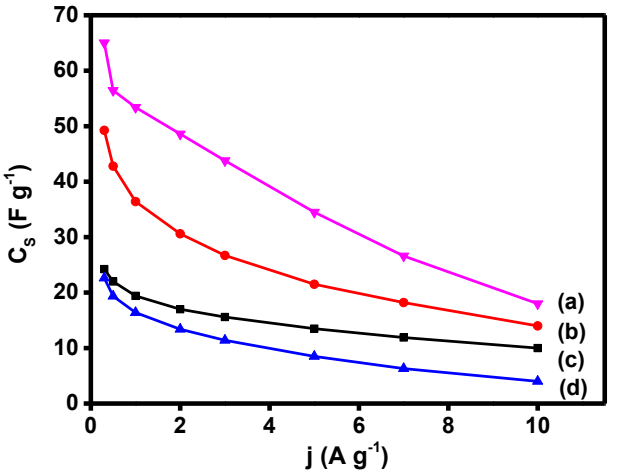

Fig. 7. C_S at current density from 0.3 – 10 A g^{-1} for (a) F-δ-MnO_2, (b) δ-MnO_2, (c) α-MnO_2 and (d) F-α-MnO_2 electrode.

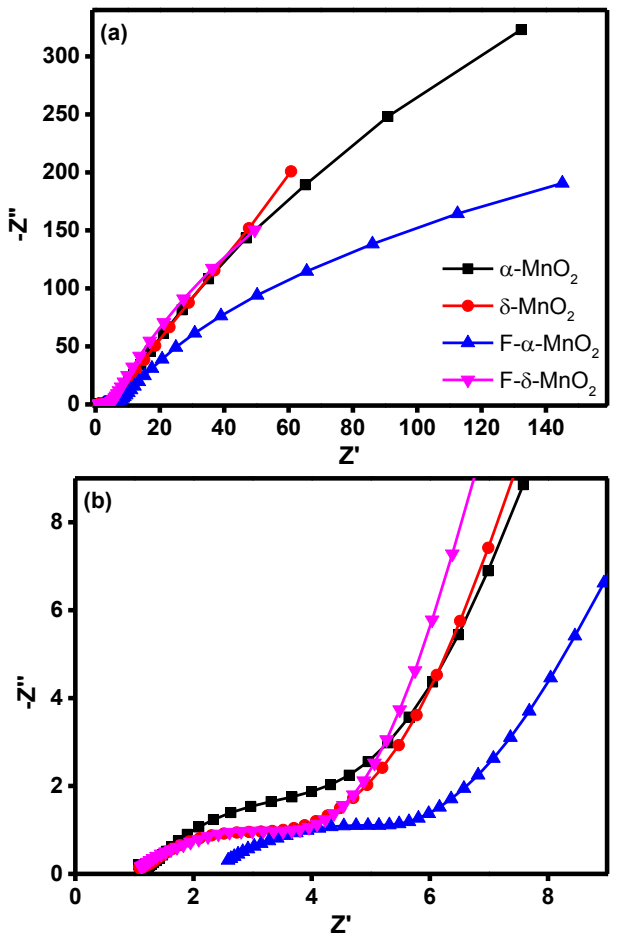

Fig. 8. (a) Nyquist plots of α-MnO_2, δ-MnO_2, F-α-MnO_2, and F-δ-MnO_2 and (b) magnified portion showing the semicircle at the high-mid frequency region.

The magnitude of the charge transfer resistance (R_{ct}) can be derived from diameter of the semi-circle. The estimated *Rct* values are 2.63, 2.51, 2.67 and 2.43 Ω for

α-MnO_2, δ-MnO_2, F-α-MnO_2, and F-δ-MnO_2. The ion diffusion resistance (R_d) is due to combination of resistance to ion diffusion extracted at the first segment of the straight line of Nyquist plot. The estimated R_d values are 4.64, 4.07, 4.66 and 3.97 Ω for α-MnO_2, δ-MnO_2, F-α-MnO_2, and F-δ-MnO_2 respectively. The R_S, R_{ct} and R_d values for F-δ-MnO_2 are the smallest which demonstrate a lower electron transfer resistance, resistance of electrochemical reaction, and ion diffusion resistance compare to α-MnO_2, δ-MnO_2, and F-α-MnO_2.

4 Conclusions

Four different types of electrode materials for supercapacitors were synthesized and their electrochemical performances were evaluated in three-electrode configuration using 0.5 M K_2SO_4. Cyclic voltammetry and galvanostatic charging–discharging (CDC) analysis shows that F-δ-MnO_2 gives the highest C_S value of 183.012 F g^{-1} at scan rate of 5 mV s^{-1} and 65.04 F g^{-1} at current density of 0.3 A g^{-1}. The EIS shows that the F-δ-MnO_2 has the lowest electrode resistances and charge transfer resistance which contribute high *Cs* and the high conductivity of electrode. Hence, F-δ-MnO_2 is considered as the best electrode material for supercapacitors compared to α-MnO_2, δ-MnO_2 and F-α-MnO_2.

The authors would like to acknowledge Universiti Malaysia Pahang for the UMP Internal Grant (RDU150354).

References

[1] M.H. Kim, J.H. Yang, Y.M. Kang, S.M. Park, J.T. Han, K.B. Kim, K.C. Roh, Colloids Surf. Physicochem. Eng. Asp. **443**, 535 (2014)
[2] Y.X. Zhang, M. Kuang, X.D. Hao, Y. Liu, M. Huang, X.L. Guo, J. Yan, G.Q. Han, J. Li, J. Power Sources. **270**, 675 (2014)
[3] S.G. Krishnan, M. Harilal, I.I. Misnon, M.V. Reddy, S. Adams, R. Jose, Ceram. Int. **43**, 12270 (2017)
[4] V. Subramanian, H. Zhu, B. Wei, Electrochem. Commun. **8**, 827 (2006)
[5] I.I. Misnon, R. Jose, New J. Chem. **41**, 6574 (2017)
[6] B.L. Vijayan, S.G. Krishnan, N.K.M. Zain, M. Harilal, A. Yar, I.I. Misnon, J.O. Dennis, M.M. Yusoff, R. Jose, Chem. Eng. J. **327**, 962 (2017)
[7] M. Harilal, S. G. Krishnan, A. Yar, I.I. Misnon, M.V. Reddy, M.M. Yusoff, J. Ojur Dennis, R. Jose, J. Phys. Chem. C. (2017)
[8] X. Zhang, X. Chang, N. Chen, K. Wang, L. Kang, Z. Liu, J. Mater. Sci. **47**, 999 (2012)
[9] S.C. Pang, S.F. Chin, C.Y. Ling, J. Nanomater. **2012**, 1 (2012)
[10] H.Y. Lin, Y.P. Sun, B.J. Weng, C.T. Yang, N.T. Suen, K.H. Liao, Y.C. Huang, J.Y. Ho, N.S. Chong, H.Y. Tang, Electrochimica Acta. **52**, 6548 (2007)
[11] Z. Li, Z. Liu, D. Li, B. Li, Q. Li, Y. Huang, H. Wang, J. Mater. Sci. Mater. Electron. **26**, 353 (2015)
[12] Y.S. Lee, *Adanced Fluoride-Based Materials for Energy Conversion* (Elsevier, Amsterdam,2015)
[13] J. Zang, X. Li, J. Mater. Chem. **21**, 10965 (2011)
[14] P.K. Nayak, T.R. Penki, N. Munichandraiah, J. Electroanal. Chem. **703**, 126 (2013)
[15] I.I. Misnon, R.A. Aziz, N.K.M. Zain, B. Vidhyadharan, S.G. Krishnan, R. Jose, Mater. Res. Bull. **57**, 221 (2014)
[16] X. Wang, A. Yuan, Y. Wang, J. Power Sources. **172**, 1007 (2007)